Volume 1
Number 5
September 2023
Pages 583–786

EES Catalysis

rsc.li/EESCatalysis

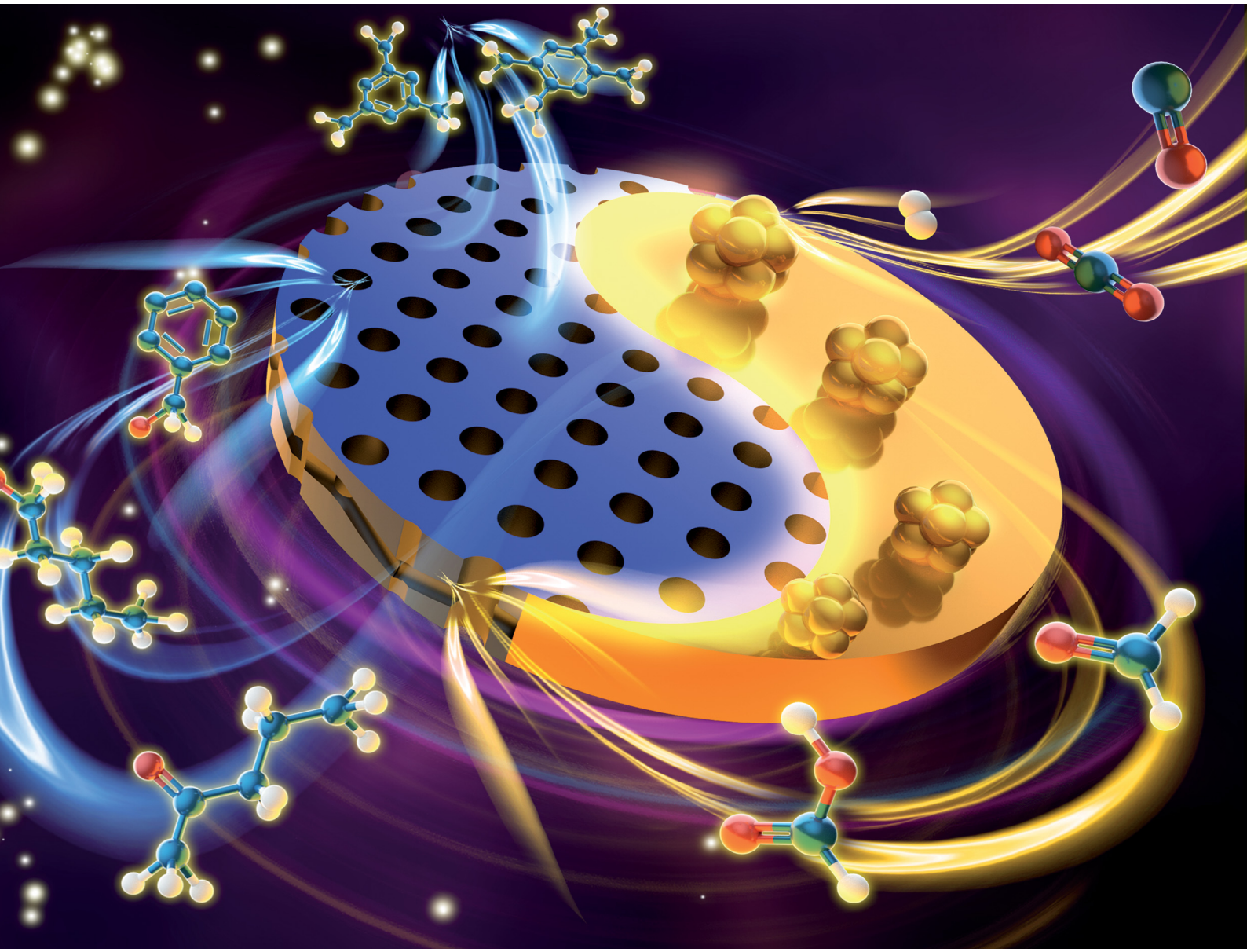

ISSN 2753-801X

ROYAL SOCIETY OF CHEMISTRY

PERSPECTIVE
Chenxi Zhang, Fei Wei *et al.*
A perspective of CO_x conversion to aromatics

EES Catalysis

PERSPECTIVE

View Article Online
View Journal | View Issue

Cite this: *EES Catal.*, 2023, 1, 677

A perspective of CO_x conversion to aromatics

Guo Tian,† Xiaoyu Liang,† Hao Xiong, Chenxi Zhang * and Fei Wei *

Received 10th May 2023,
Accepted 26th June 2023

DOI: 10.1039/d3ey00102d

rsc.li/eescatalysis

The sustainable production of chemicals through CO_x hydrogenation is a growing area of interest, with thermal catalytic conversion showing the most promise. Selective hydrogenation to high carbon number products (C_{8+}) remains a challenge, and this perspective focuses on recent advancements in heterogeneous catalytic CO_x hydrogenation to aromatics. Efficient conversion has been achieved using tandem catalysts composed of metal oxides and nano-porous zeolites, particularly H-ZSM-5, which activate CO_x and dissociate H_2 while promoting precise C–C coupling and cyclization. Such behavior facilitated the system towards a simple biological system. However, understanding the reaction mechanisms, including product selectivity and catalyst activity regulation is still a challenge. This perspective reviews recent progress and integrates quantitative activity descriptors for metal-dependent speciation within the biological metabolic system. H* adsorption energy in the presence of C_1 oxygenate intermediates is identified as a speciation-sensitive activity descriptor, while zeolite topologies serve as product selectivity descriptors. These findings establish robust structure–performance relationships and guide the rational design of high-performance CO_x hydrogenation to aromatic catalysts.

Broader context

In the burgeoning field of CO_x hydrogenation for sustainable chemical production, thermal catalytic conversion stands out as the most promising avenue. This perspective emphasizes recent strides made in selective hydrogenation to higher carbon number products (C_{8+}) *via* heterogeneous catalytic CO_x hydrogenation to aromatics, a challenge that remains at the forefront of the field. Notably, substantial conversion efficiency has been realized through the employment of tandem catalysts, specifically metal oxides, and nano-porous zeolites like H-ZSM-5. These catalysts activate CO_x and dissociate H_2, simultaneously fostering precise C–C coupling and cyclization, and thereby drawing parallels to simple biological systems. Nevertheless, fully deciphering the reaction mechanisms, including aspects of product selectivity and catalyst activity regulation, remains a daunting task. This perspective integrates the recent breakthroughs and introduces quantitative activity descriptors for metal-dependent speciation in relation to the biological metabolic system. It pinpoints the H* adsorption energy in the presence of formyl as a key activity descriptor sensitive to speciation, while zeolite topologies emerge as significant product selectivity descriptors. These insights solidify structure–performance relationships and illuminate the path towards rational design of high-performance catalysts for CO_x hydrogenation to aromatics.

Introduction

In the realm of sustainable chemical production, the hydrogenation of CO_2 or CO (collectively known as CO_x) to generate value-added compounds has attracted considerable interest.[1–3] Numerous reviews have delved into the heterogeneous catalytic hydrogenation of CO_x, examining techniques such as thermal, electrochemical, and photochemical processes.[4,5] While each approach possesses promise, thermal catalytic conversion exhibits superior yields and scalability. Recent advancements have facilitated the synthesis of oxygenates (*e.g.*, CH_3OH and C_2H_5OH), light olefins ($C_{2-4}^{=}$), gasoline (C_{5+}), and heavy aromatics (C_{8-12}) using CO_x as a feedstock.[6,7] Nevertheless, the selective hydrogenation of CO_x to high carbon number products (C_{8+}) remains a formidable challenge due to unpredictable C–C coupling and a multitude of elementary reactions.

Aromatic compounds characterized by a low H/C ratio (1 : 1–1 : 1.5), similar to biomass-derived feedstocks, may represent an ideal outcome from renewable pathways (Fig. 1(a)). Furthermore, the limited H_2 consumption capacity could yield substantial economic value (Fig. 1(b)). In comparison to conventional hydrocarbons and oxygenates, the favorable thermodynamic driving force at low temperatures offers superior energy conservation and lays the groundwork for rational catalyst design (Fig. 1(c)). Generally, the entropy contribution arising from mixed products results in more favorable Gibbs free energy than that of most individual products (Fig. 1(d)). This observation offers a unique perspective on the production of high-quality synthetic fuels rather than single fine chemicals. The escalating global demand

Beijing Key Laboratory of Green Chemical Reaction Engineering and Technology, Department of Chemical Engineering, Tsinghua University, Beijing, China 100084. E-mail: wf-dce@tsinghua.edu.cn, cxzhang@tsinghua.edu.cn
† These authors contributed equally to this work.

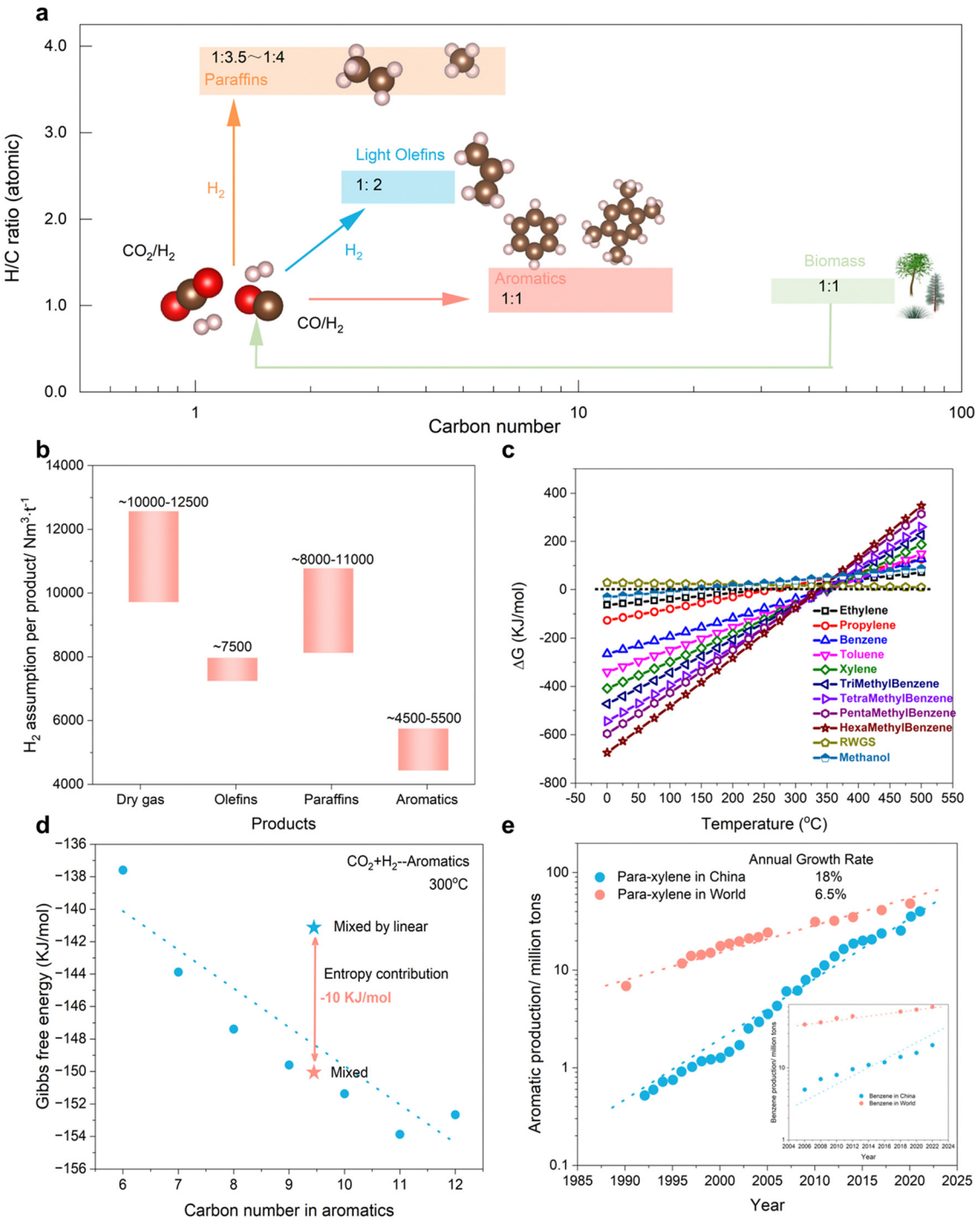

Fig. 1 Economic and atomic analysis of CO_x conversion to aromatics *versus* other hydrocarbons. (a) Atomic and economic analysis of CO_x conversion to paraffins, light olefins and aromatics. (b) H_2 assumption profile over typical hydrocarbons. (c) Thermodynamical equilibrium of CO conversion to hydrocarbons and oxygenates. (d) Gibbs free energy of mixed aromatics *versus* single aromatic products. (e) Some typical aromatic productivity in the world *versus* China.

for aromatic compounds necessitates alternative production routes beyond petroleum-based methods (Fig. 1(e)). Based on the aforementioned acknowledgements, our perspective focuses on the heterogeneous catalytic hydrogenation of CO_x to aromatics, highlighting the reaction mechanisms responsible for generating these valuable materials. Our efforts aim to bridge the knowledge gap and guide researchers in this field towards the development of more efficient and selective catalysts.

The proficient transformation of CO_x to heavy aromatics has been accomplished *via* the utilization of tandem catalysts, specifically comprising metal oxides and nano-porous zeolites, with H-ZSM-5 being particularly noteworthy.[8] In this arrangement, the

metal oxides function to activate CO_x and dissociate H_2, while the confined acidic pores of H-ZSM-5 facilitate accurate C–C coupling and cyclization.[9] Intriguingly, the tailored diameter pores of H-ZSM-5, possessing a dynamic diameter compatible with benzene, toluene, and xylene (BTX), result in heightened aromatic selectivity.[10] Following this, surface methylation of BTX transpires at the exterior surface of H-ZSM-5, forming heavy aromatics (C_{8+}), with CH_3O^* generated on the metal oxide surface, a mechanism widely acknowledged by researchers.[11,12] Moreover, an acid–base heterostructure formed by the close proximity between metal oxides and H-ZSM-5 ensures the rapid diffusion of key intermediates originating from the metal oxides.[13,14] This catalytic process bears similarity to a rudimentary one,[15] wherein the transfer of matter (C–C coupling) and energy (thermodynamic driving force) is optimized. Nonetheless, despite its potential, a significant challenge lies in developing a comprehensive understanding of the metabolic system and establishing an activity and selectivity descriptor to accurately delineate its catalytic behavior.

A multitude of unresolved questions persist regarding the diverse reaction mechanisms implicated in catalysts for CO_x hydrogenation to aromatics, encompassing aspects such as product selectivity, catalyst activity regulation, and the enhancement of catalytic performance. The fundamental challenge associated with these catalysts remains a crucial research focus. Despite employing an array of methods, including *in situ* IR, NMR, and synchrotron-based photoionization mass spectrometry, the actual mechanism remains highly contentious.[16] The intricacy of coexistent species, coupled with the elevated reaction temperatures and pressures necessitated for certain steps, frequently results in active and low-concentration intermediates, further exacerbating the issue and rendering most techniques inadequate for detecting these elusive species. Such disputes surrounding the mechanism have significantly impacted the advancement and comprehension of next-generation high-performance catalysts.

In this perspective, we comprehensively review recent advancements in CO_x hydrogenation to aromatics, integrating these developments to derive quantitative activity descriptors that account for metal-dependent speciation within this biological metabolic system. Moreover, through in-depth multivariate analysis, we investigate the chemistry involved in different zeolite topologies when combined with highly active oxide-based catalysts for CO_x hydrogenation to olefins, aromatics, and paraffins. By combining kinetic, transient, and chemisorption analyses with modelling, we identify H^* adsorption energy in the presence of C_1 oxygenate intermediates as a speciation-sensitive activity descriptor, while zeolite topologies serve as product selectivity descriptors. These findings are crucial in establishing robust structure-performance relationships and guiding the rational design of next-generation, high-performance CO_x hydrogenation to aromatic catalysts.

Results and discussion

Activity side on the metal oxides

In general, the thermodynamic driving force of mixed aromatic products is more favorable than that of single aromatics. Additionally, mixed aromatic products with carbon numbers ranging between C_{8-12} may also serve as aviation fuel additives.[17,18] Consequently, recent studies have primarily concentrated on synthesizing mixed aromatic products. Within the domain of thermocatalytic hydrogenation of CO_x to aromatics, metal oxides are pivotal in activating CO_x and dissociating H_2.[19,20] Two categories of metal oxides have been investigated for this process: Fischer–Tropsch-based oxides, such as Fe, Co, and Mo, and spinel-type metal oxides rich in oxygen vacancies.[21] The Fischer–Tropsch categories combining the Fischer–Tropsch-based oxides with the zeolite can achieve a high CO single pass conversion with moderate aromatics selectivity. Ma *et al.*[6] exploited a combination of Na–Zn–Fe_5C_2 and hierarchical HZSM-5 showed a high selectivity of aromatics of 51% under the stable stage with CO conversion over 85%. Although the addition of zeolite can break the Anderson–Schulz–Flory (ASF) distribution of Fisher–Tropsch synthesis to a certain extent, the formation of C–C bonds at the metal oxide is still not well controlled, resulting in limited selectivity of aromatics.

In contrast, the spinel-type metal oxides rich in oxygen vacancies are particularly fascinating, as they circumvent the Anderson–Schulz–Flory rule limitation and exhibit enhanced selectivity towards target aromatics when paired with H-ZSM-5, which exerts significant constraint effects.[22] Therefore, numerous researchers have concentrated on developing highly effective metal oxide + H-ZSM-5 composite catalysts. Examples of these composite catalysts include $ZnAl_2O_4$, $ZnCr_2O_4$, and $ZnZrO_x$, which can generate C_1 oxygenates from CO_x hydrogenation and subsequently transform them into aromatics utilizing the H-ZSM-5 component.[23] Various studies have revealed that, in this biological metabolic system, catalytic activity is predominantly constrained by the metal oxide aspect. Without compromising aromatic selectivity, considerable efforts have been dedicated to enhancing the capacity of CO_x conversion over traditional spinel-based metal oxides.

In a recent study, Wang and colleagues shed light on the advantageous effects of heteroatom doping, including Al, Ce, Zn, Mo, and Pt, into ZrO_2 catalysts on H_2 adsorption and dissociation.[24] Their research showcased the significant impact of these modifications on the catalytic performance of syngas to aromatics when combined with H-ZSM-5, as depicted in Fig. 2(a). These findings suggested that the d-band electrons of metals could be tuned while preserving the catalyst structure, resulting in effective regulation of reaction activity primarily controlled by the metal oxide side. A similar approach was adopted by Wei *et al.*,[25] introducing appropriate amounts of F–T metals, such as Fe and Co, into spinel-type $ZnCr_2O_4$ to significantly improve CO conversion without sacrificing total aromatic selectivity, as depicted in Fig. 2(b). To evaluate the ability of doping metals for CO_x and H_2 activation, Wang *et al.* conducted H_2–D_2 exchange studies for M-ZrO_2 catalysts, as well as pristine ZrO_2, as depicted in Fig. 2(c). They deduced that metals with moderate H_2 activation energy, such as Zn and Mo, are an ideal choice to balance the trade-off between activity and target product selectivity. Additionally, Wei *et al.*[25] carried out density functional theory calculations (DFT) to quantitatively evaluate CO adsorption and H_2 dissociation energy. As shown

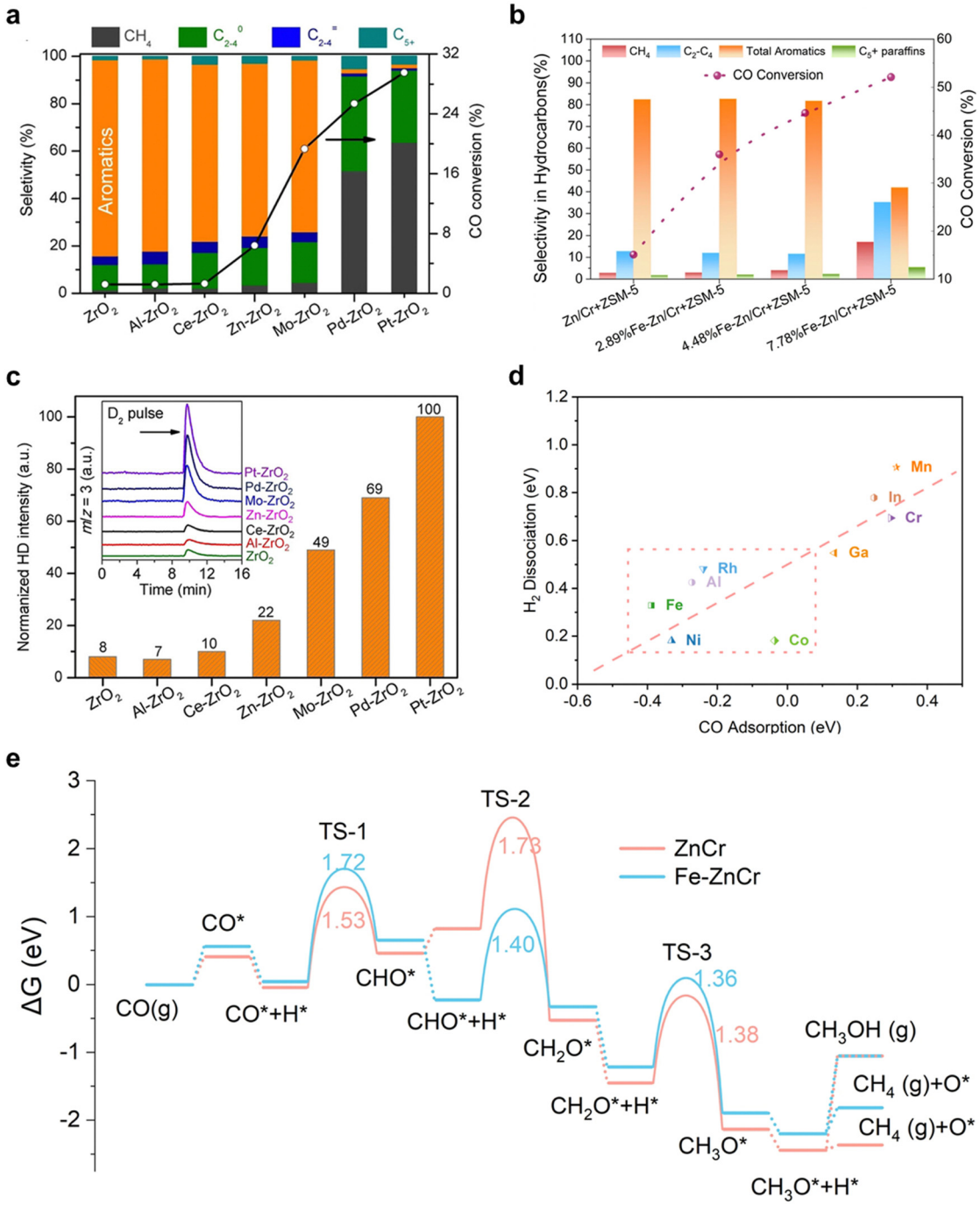

Fig. 2 The modulation on metal oxides in syngas to aromatics. (a) Effect of metal doping on the catalytic performance of M-ZrO_2/H-ZSM-5 (M denotes metal oxides). Reprinted with permission. Copyright 2019 Chemistry Europe. (b) Catalyst evaluation of pristine $ZnCr_2O_4$ and different Fe–Zn/Cr with H-ZSM-5. Reprinted with permission. Copyright The Author(s) 2022. (c) Normalized HD formation rate over M-ZrO_2. Reprinted with permission. Copyright 2019 Chemistry Europe. (d) H_2 dissociation energy *versus* CO adsorption over different M-ZnCr catalysts. (e) Gibbs free energy diagrams of syngas conversion to CH_3OH/CH_4 on pristine and Fe/ZnCr(111) surfaces with 1/4 ML O_v. Reprinted with permission. Copyright The Author(s) 2022.

in Fig. 2(d), matched CO adsorption energy with H_2 dissociation is speculated to achieve high performance CO_x to aromatics. Overall, the results and analysis suggest that measuring the CO_x adsorption and H_2 dissociation ability is a feasible method for evaluating metal oxides, further enabling high-throughput screening for suitable metals.

In a recent study, Wei *et al.*[25] employed density functional theory (DFT) calculations to examine the reaction pathway of CO hydrogenation, as depicted in Fig. 2(e). CO adsorption takes place at O_v, succeeded by H_2 dissociation near the surface O_v and H* adsorption on an O situated in proximity to 16d site metals. The CO* then undergoes progressive hydrogenation,

forming CHO*, CH_2O*, CH_3O*, and ultimately CH_3OH/CH_4. The authors discovered that on pristine $ZnCr_2O_4$ (111) with O_v, H* formation is impeded due to the presence of CHO* and the robust adsorption of CH_3O*. Conversely, the integration of isolated Fe stabilizes the state of CHO* + H*, rendering the hydrogenation step to produce H_2CO* energetically exothermic while destabilizing the state of CH_2O* + H*, thereby promoting CH_3O* formation. As illustrated in Fig. 2(e), the generation of CH_3OH and CH_4 diverges from CH_3O* on the oxide catalysts, both being endothermic with reaction energies as high as 1.14 and 0.38 eV, respectively, and less thermodynamically viable than the preceding endothermic steps to form H_2CO*/CH_3O* from CO. Furthermore, earlier theoretical investigations propose that the hydrogenation of CH_3O* to CH_3OH or CH_4 presents the highest kinetic barrier.[26,27] Consequently, Fe doping can enhance CO conversion, resulting in the production of significant quantities of CH_4, suggesting that Fe aids in the transformation of syngas to an intermediate capable of rapid conversion to CH_4. H-ZSM-5 is subsequently necessary for the further alteration of the intermediate. Wei *et al.* posited that the intermediate is CH_3O*/CH_2O*, which has recently been successfully identified in an experiment by Hou *et al.*[28]

In consideration of recent investigations on metal oxides in tandem biological metabolism systems, we have assembled evidence signifying that the activity of CO_x hydrogenation to aromatics is predominantly constrained by metal oxide properties, specifically, the activation of CO_x and H_2 dissociation capability. Furthermore, we have ascertained that the formation rate of CH_2O* represents the rate-limiting step within the extensive reaction pathway. To tackle this, we put forward a quantitative activity

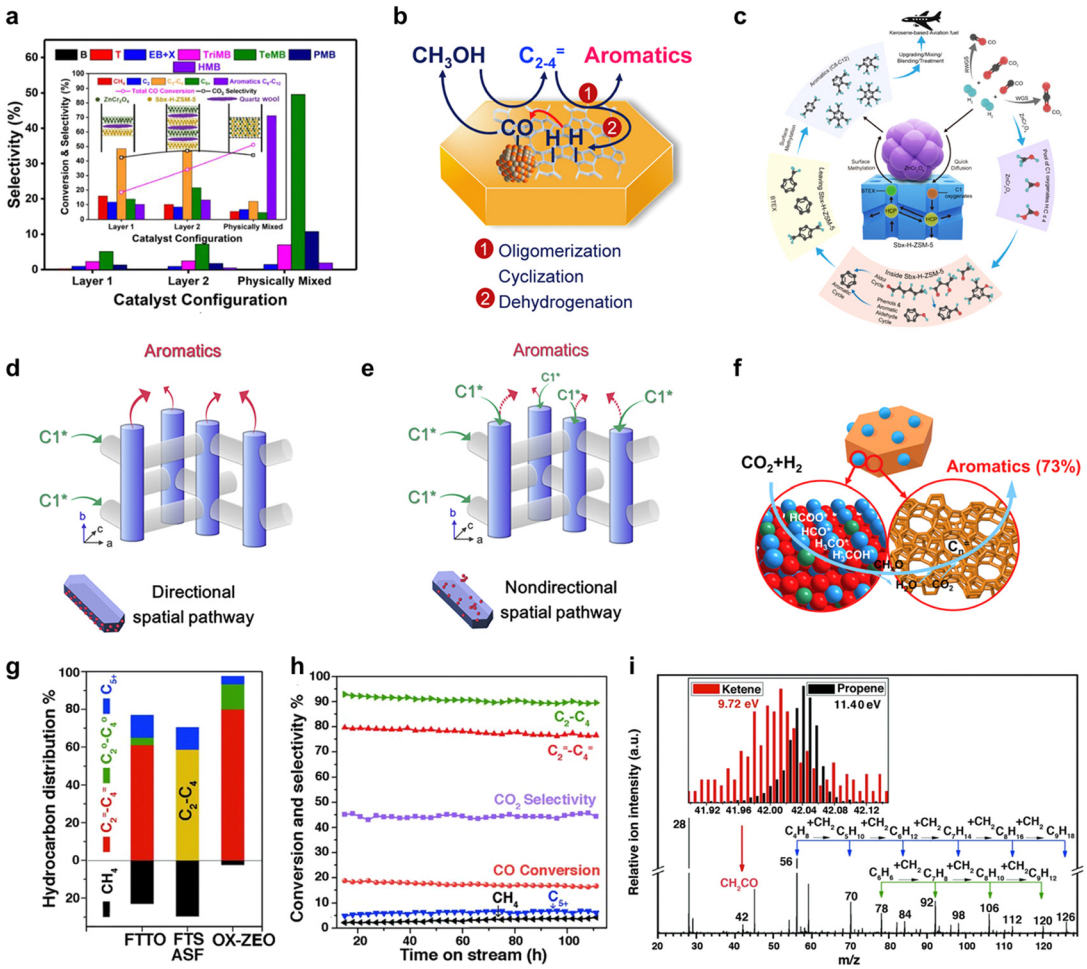

Fig. 3 The identification of key intermediates and their diffusion ability over bifunctional catalysts. (a) Product distribution and catalytic activity in different catalyst placement orientations. Reprinted with permission. Copyright 2020 American Chemical Society. (b) Schematic of the proposed reaction mechanism of CO_2 hydrogenation on the tandem catalyst. Reprinted with permission. Copyright 2017 Elsevier Inc. (c) Functioning mechanism of diffusion ability of CH_3OH into H-ZSM-5. Reprinted with permission. Copyright 2022 American Chemical Society (d) and (e) comparison between the directional and nondirectional spatial pathway for tandem reaction of syngas to aromatics; (d) directional spatial pathway and (e) nondirectional spatial pathway, C1* represents C1 intermediate. Reprinted with permission. Copyright 2021 Elsevier Inc. (f) Proposed reaction mechanism for the highly selective conversion of CO_2 or syngas into aviation fuel precursors over the nano-sized bifunctional catalyst $ZnCr_2O_4$/H-ZSM-5. Reprinted with permission. Copyright 2018 Elsevier Inc. (g) and (h) The catalyst performance in syngas to light olefins. Reprinted with permission. Copyright 2016, American Association for the Advancement of Science. (i) *In situ* study of syngas conversion over $ZnCrO_x$ with CH_2CO as a key intermediate by SVUV-PIMS. Reprinted with permission. Copyright 2016, American Association for the Advancement of Science.

descriptor of H* adsorption energy in the presence of C_1 oxygenate intermediates. By modulating the d-band center of metal oxides, we can effectively regulate the adsorption energy of key intermediates and accelerate the reaction towards desired products.

Surface diffusion of key intermediates

It is widely acknowledged that C1 oxygenates predominantly form on the surface of metal oxides. The diffusion of C1 oxygenates into the acidic pores of H-ZSM-5 may establish a bridge connecting two distinct reactions.[29] The crucial role of key intermediate diffusion between catalyst A and catalyst B in tandem catalytic systems is well-established, necessitating a comprehensive examination of the system's configuration to understand its catalytic behavior. Up to this point, active site proximity between catalyst A and catalyst B has primarily been dictated by particle size or catalyst arrangement.[30,31] Guided by these insights, numerous investigations have been undertaken to explore the surface diffusion propensity within this framework.

As illustrated in Fig. 3(a), differing catalyst placement orientations yield distinct catalytic performances and product distributions in syngas-to-aromatics conversion. Physically mixed composite catalysts exhibit notably improved aromatics selectivity and CO conversion in comparison to separated/layered catalyst orientations. Analogous observations are documented in Xu *et al.*'s[32] research utilizing a Ce–Zr/ZSM-5 catalyst and Wang *et al.*'s[19] investigation employing a Zn–ZrO_2/H-ZSM-5 catalyst, both suggesting that decreased catalyst particle size, resulting in closer proximity, leads to heightened aromatics selectivity. These findings collectively emphasize the vital role of intermediate diffusion between the bifunctional catalyst's two active components in tandem reaction product distribution. Fig. 3(b) portrays the influence of surface diffusion on the tandem reaction, where intermediates formed on the metal oxide side transfer to the zeolite side for further conversion to aromatics, and H species from aromatics formation return to the metal oxide side for CO hydrogenation. In addition to the diffusion of C_1 intermediates and H species, the diffusion of aromatics bears considerable significance. As depicted in Fig. 3(c), Wei *et al.*'s study[33] discloses that short *b*-axis nano ZSM-5 surfaces with $ZnCr_2O_4$ attachment display superior desorption capabilities compared to those lacking $ZnCr_2O_4$, while the desorption ability of phenol exhibits an opposite trend. This asymmetric desorption in bifunctional catalysts contributes to heightened tandem reaction catalytic performance. Such behaviors indicate the existence of dual transfer in this tandem system, which profoundly affects the catalytic performance.

Intermediates and product diffusion can be directionally modulated by designing the proximity of bifunctional catalysts in an oriented manner. As depicted in Fig. 3(d) and (e), Xie *et al.*[34] introduced a directional-diffusion catalyst featuring a highly exposed (010) ZSM-5 surface and preferentially attached Cr_2O_3 to (100) and (101) surfaces *via* a recrystallization method. This arrangement facilitates C_1 intermediates, generated on metal oxide sites, to likely diffuse into adjacent sinusoidal channels of ZSM-5, while enabling aromatic products to easily diffuse out through straight channels. The directional pathway resulted in a striking enhancement in catalytic performance. Regarding CO_2 conversion to aromatics, surface diffusion of key intermediates also plays a pivotal role. Analogous to the CO-to-aromatics conversion, CH_xO species generated on the metal oxide side through CO_2 hydrogenation are transferred to the zeolite side for further conversion to aromatics.[35] Notably, catalyst performance exhibits pronounced differences depending on the proximity between the active components. Beyond CO_x-to-aromatics conversion, intermediate diffusion assumes a significant role in this tandem system, such as the transformation of CO_x to light olefins. As illustrated in Fig. 3(g)–(i), CH_2CO, generated from CO hydrogenation, serves as the key intermediate in the tandem reaction, as detected by highly sensitive synchrotron-based vacuum ultraviolet photoionization mass spectrometry (SVUV-PIMS).[7,36] Through surface diffusion, intermediates reach the MSAPO side and subsequently convert to light olefins under the selective catalysis of zeolite.

Considering recent advancements in zeolite research within tandem biological metabolism systems, it is evident that surface transfer of key intermediates establishes a crucial connection between the CO_x active reaction on the metal oxide side and the selective production of target products on the zeolite side. By modulating the proximity of active components and designing the diffusion pathway, both CO_x conversion and target product selectivity can be significantly enhanced.

Selectivity side on the zeolites

While the H* adsorption energy with the existence of C_1 oxygenate intermediates is a speciation-sensitive activity descriptor, zeolite topologies act as a product selectivity descriptor.[30,37] Several studies have demonstrated that in this biological metabolic system, the product distribution mainly depends on the side of the zeolite. Through the surface diffusion, the C_1 oxide intermediates, generated from CO_x catalyzed by metal oxide, enter the zeolite pore, which acts as a selective reaction vessel and are further transformed into target products through carbon chain growth, dehydrogenation, cyclization, *etc.*[38] Various pore zeolite topology structures with different pore sizes and cage structures, show unique domain limiting effects leading to diverse product selectivity. So that when metal oxides are coupled with different zeolites, the restriction of thermodynamics can be broken and different target products can be obtained with high selectivity.

SAPO-34, featuring a CHA framework type, possesses an ellipsoidal cage (1.1 × 0.65 nm) and forms a three-dimensional pore structure through six eight-membered rings, with a pore size of 3.8 Å.[39] This narrow pore allows passage of only small molecules and hydrocarbons, while restricting diffusion of long-chain hydrocarbons and larger aromatic molecules.[40] As a result, SAPO-34 serves as a common catalyst for the targeted synthesis of light olefins ($C_{2-4}^{=}$). Bao *et al.*[7] utilized OX-ZEO and combined the $ZnCrO_x$ with MSAPO to achieve the conversion of syngas to C_{2-4} with the selectivity up to 94% at a CO conversion of 17%. Recently, Li *et al.*[41] developed a ZnZrO/SAPO-34 tandem catalyst that combines a ZnO–ZrO_2 solid

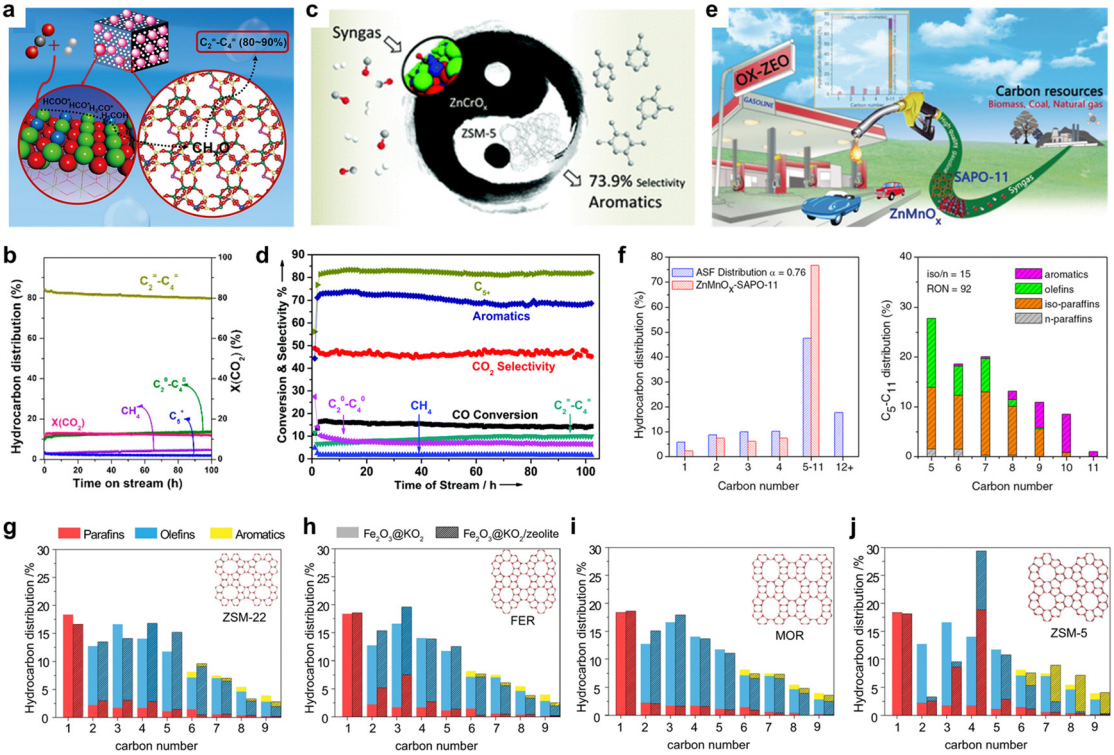

Fig. 4 Different catalytic performances over bifunctional catalysts. (a) Schematic of the proposed reaction mechanism of CO_2 hydrogenation to light olefins. Reprinted with permission. Copyright 2017 American Chemical Society. (b) Catalytic performance over ZnO–ZrO_2/SAPO-34. Reprinted with permission. Copyright 2017 American Chemical Society. (c) Schematic of the proposed reaction mechanism of CO_2/CO hydrogenation to aromatics. Reprinted with permission. Copyright The Royal Society of Chemistry 2017. (d) Catalytic performance over ZnO–ZrO_2/H-ZSM-5. Reprinted with permission. Copyright The Royal Society of Chemistry 2017. (e) Schematic of the proposed reaction mechanism of CO hydrogenation to gasoline. Reprinted with permission. Copyright 2019 Wiley-VCH VerlagGmbH & Co. KGaA, Weinheim. (f) Catalytic performance over $ZnMnO_x$/SAPO-11. Reprinted with permission. Copyright 2019 Wiley-VCH VerlagGmbH & Co. KGaA, Weinheim. (g)–(j) Detailed hydrocarbon distribution for selected zeolite frameworks in a dual-bed configuration during Fe_2O_3@KO_2/zeolite bifunctional material catalyzed hydrogenation of CO_2. Reprinted with permission. Copyright The Author(s) 2021.

solution with a Zn-modified SAPO-34 zeolite, as depicted in Fig. 4(a) and (b). By leveraging the constraining effect of SAPO-34, the selectivity for lower olefins reaches 80–90% among hydrocarbon products under conditions of 380 °C, 2 MPa, and 3600 ml g_{cat}^{-1} h^{-1}. Furthermore, this catalytic performance can be sustained over 100 h under the same conditions, laying the groundwork for its industrialization. Similar results can be achieved under the catalysis of In_2O_3/ZrO_2/SAPO-34[42] or In_2O_3–$ZnZrO_x$/SAPO–34.[43]

Owing to the well-matched straight channel of H-ZSM-5 (5.6 × 5.3 Å) with the dynamic diameter of benzene, toluene, and xylene (BTX), employing H-ZSM-5 with an MFI structure as the selectivity component enables the direct conversion of CO_x to aromatics.[44] As illustrated in Fig. 4(c) and (d), Wang *et al.*[19,45] achieved an aromatics selectivity of ~80% at a single-pass CO conversion of 16.0%. It should be noted that, due to the strong external acidic properties of H-ZSM-5, BTX undergoes alkylation reactions at the (010) surface of H-ZSM-5 to form heavier aromatics such as tri- or tetra-methylbenzene. Recently, Wei *et al.*[33] accomplished the conversion of CO_2 to high-energy-density aviation fuel, polymethyl benzene (C_{10+}), with high selectivity by employing short *b*-axis ZSM-5 with superior specific surface area and diffusion properties. Tsubaki *et al.* achieved highly selective preparation of PX by modifying ZSM-5 with silica[46] or employing tailor-made ZSM-5[47] to reduce the acidic sites on the external surface of the zeolite.

Furthermore, similar strategies for designing product-oriented catalysis have also been adopted by researchers in this field. Bao *et al.*[48] explored zeolites with 1D ten-membered-ring (10-MR) channel structures, such as SAPO-11 and ZSM-22, combined with $Zn_aMn_bO_x$. This approach facilitated the direct conversion of syngas into C_{5+} gasoline, achieving a selectivity of 76.7% among hydrocarbons at a 20.3% CO conversion, as depicted in Fig. 4(e) and (f). Generally, this catalytic process exhibits a longer lifetime compared to traditional methanol conversion to gasoline, light olefins, or aromatics, owing to the facile diffusion properties of the final products facilitated by the synergistic effect between metal oxides and zeolites.[49]

The substantial influence of zeolite topology on reaction product distribution has garnered the attention of several researchers. Abhishek Dutta Chowdhury *et al.*[37] investigated zeolite as a descriptor governing ultimate product selectivity. In their study, eight zeolite catalysts, including MOR, SAPO-34, ZSM-58, BETA, Y, FER, ZSM-22, and ZSM-5, were tested for CO_2 conversion, with Fe_2O_3@KO_2 remaining constant as the metal oxide on the activity side, as depicted in Fig. 4(g)–(j). The results

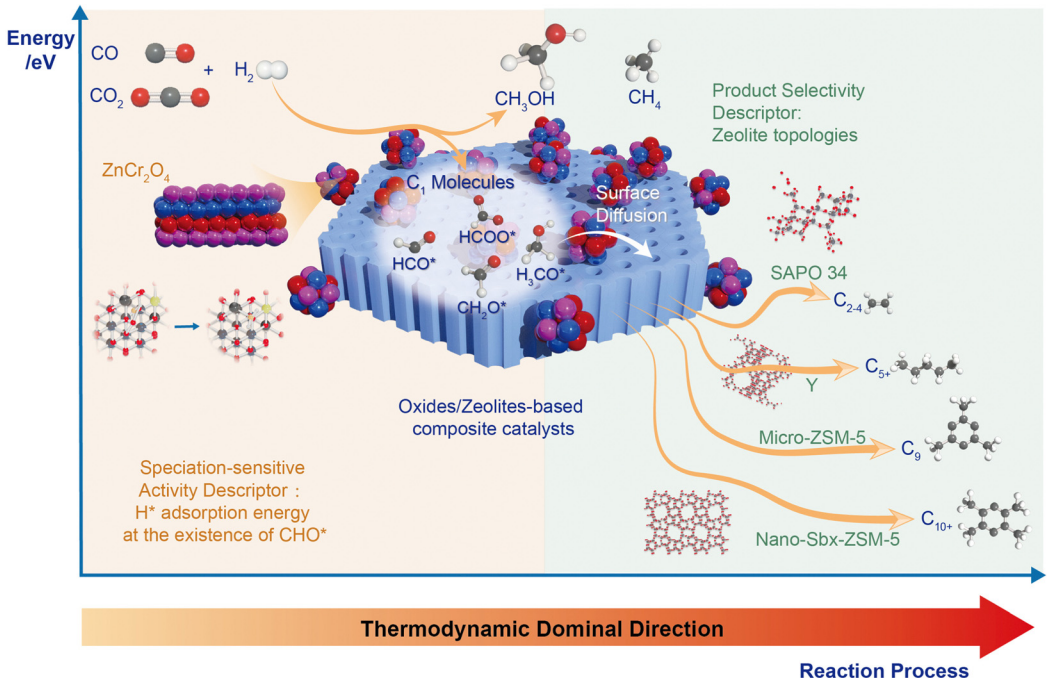

Fig. 5 Schematical diagram of bifunctional catalysts and corresponding activity and selectivity descriptor.

reveal that different zeolites yield vastly distinct product distributions, while CO_2 conversion remains nearly constant. MOR exhibits exceptional diffusion performance, resulting in high selectivity for $C_{2-4}^{=}$. Conversely, ZSM-22 with 1D, 10MR and FER with 2D, 10MR facilitate the targeted synthesis of $C_{5-9}^{=}$ and C_{2-9}, respectively, due to the linear expansion effect. Moreover, ZSM-5 demonstrates outstanding aromatic selectivity. The combined outcomes of experimental and computational analyses highlight the vital role played by the hybrid nature of the active zeolite catalyst, its preferred CO_2-derived reaction intermediates, and zeolite topology in determining the ultimate product selectivity. Recent studies on zeolites in tandem biological metabolism systems have revealed that product distribution is predominantly constrained by the zeolite. By judiciously selecting zeolites and further refining their topological structures and acid sites, it is possible to achieve higher selectivity for the desired product.

Conclusion

Based on recent research on zeolites in tandem biological metabolism systems, we propose that the tandem reaction proceeds *via* the following steps (Fig. 5): (1) activation of CO_x on the metal oxide side, generating CH_xO intermediates through hydrogenation; (2) surface diffusion of key intermediates; and (3) selective catalysis on the zeolites.

In the first step of this tandem biological metabolism system, CO or CO_2 undergoes activation *via* stepwise hydrogenation. CO is adsorbed at O_v, followed by H_2 dissociation near the surface O_v, on an appropriate metal oxide with suitable CO adsorption and H_2 dissociation energy. The CO* then undergoes gradual hydrogenation along the pathway: CO* → CHO* → CH_2O* → CH_3O* → CH_3OH/CH_4.[50] Similarly, CO_2 activation follows a stepwise hydrogenation path with two possible pathways: the formate pathway and the carboxyl pathway.[51] The formation of the key intermediate H_2CO*, which has the highest formation energy and is easily desorbed into the gas phase, is the decisive step in the activation of both CO_2 and CO. Hence, the H* adsorption energy in the presence of C_1 oxygenate intermediates serves as the quantitative active descriptor in this step.

With the presence of zeolite, H_2CO* intermediates effectively desorb into the zeolite pore for further reaction, whereas in the absence of zeolite, these intermediates must continue hydrogenation to produce methanol or methane, which have higher reaction energy barriers. The introduction of zeolites facilitates the desorption and surface diffusion of critical intermediates, allowing the modulation of proximity between the two active components to effectively regulate diffusion, leading to dramatic changes in conversion and selectivity.

Within the acidic zeolite pore, key intermediates transferred from the metal oxide side undergo further transformation into hydrocarbons. An aldol-aromatic mechanism, supported by *in situ* spectroscopic and microscopic characterization methods and theoretical calculations, explains the reactions on the zeolite side.[33,52] This mechanism involves C–C coupling of reaction intermediates *via* aldol condensation and Prins reaction, generating crucial hydrocarbon pool species under the spatial constraints of the zeolite. Oxygenate intermediates are then converted to single-ring aromatics through hydrogenation/dehydrogenation and dehydration. The product distribution is primarily limited by the topology structures of the zeolite, with different zeolites exhibiting various pore sizes, cage structures, and acid sites. The match between the zeolite

pore size and the molecular dynamics size of the product is the fundamental factor for the differing product selectivity. In these tandem biological metabolism systems, we can store the energy of high-energy gaseous phase reactants in target hydrocarbons *via* thermochemical storage. Analyzing this system allows for directed performance improvement through appropriate control of key descriptors at each step, offering guidance for designing the next generation of CO_x transformation reactions.

Challenges and perspective

In this review, we present an in-depth analysis of tandem catalysis systems for the conversion of CO_x into aromatics and other value-added products, with a particular emphasis on heavy aromatics. While these novel tandem catalyst systems hold promise as alternatives to traditional crude oil-based production methods for aromatics, significant advancements in performance are still required. A critical aspect of this endeavor involves elucidating the underlying mechanisms within the ''black box'' where the actual catalysis occurs. Specifically, identifying descriptors that connect micro-scale characteristics such as adsorption and activation energy with macro-scale performance indicators like reactant conversion and product selectivity is crucial. As we navigate this dynamic landscape, we are met with both immense opportunities and formidable challenges in the pursuit of sustainable and efficient catalytic systems.

First of all, in the context of CO_x to aromatics conversion processes, thermodynamical constraints present a significant challenge. Mixed aromatics, in particular, are less thermodynamically restricted at lower temperatures. Nevertheless, the extensive chain-growth and aromatization reaction pathway required for the reduction of inert CO_2 demands a considerable energy input, necessitating high temperatures. As a result, the development of high-activity catalysts that can operate effectively at low temperatures is crucial for the advancement of this field. One viable approach is to introduce high activity metals such as Fe, Mo, Pt, *etc.* into the metal oxides while avoiding the C–C coupling. By addressing these thermodynamic hurdles, we can tap into the full potential of these processes and foster more efficient and sustainable production strategies for aromatics.

Secondly, the unique attributes of aromatics as self-catalyzed ring-terminated carbons with fewer than 12 carbon atoms position them as essential high-carbon building blocks in modern chemical and material industries. These inherent properties enable the circumvention of challenges associated with product selectivity and hydrogen consumption, which commonly arise from the Anderson–Schulz–Flory (ASF) distribution. By concentrating research efforts on these high-carbon components, the scientific community can propel the development and optimization of conversion processes. Nonetheless, most catalysts in this system are prone to carbon deposition, leading to a decline in catalytic performance. Consequently, extending the lifetime of this innovative catalysis system from hundreds to thousands of hours is imperative for enhancing its practicality and viability. This advancement, in turn, will establish more efficient and accurate production methods for valuable aromatic compounds, further solidifying their significance and applications across various sectors.

Thirdly, the intricate structure of metal oxides and zeolites presents an intriguing area of study. Under a reduction atmosphere (CO, CO_2, H_2), the physical mixture of metal oxides and zeolites may undergo dynamic structural evolution, leading to the formation of heterostructures. Unraveling the interface between metal oxides and zeolites and its capacity for key intermediate diffusion remains a challenge. It is anticipated that density functional theory (DFT) studies, in conjunction with highly sensitive *in situ*/operando spectroscopic techniques, can offer more profound insights. Deciphering the high efficiency of this catalytic performance, conferred by the complex catalytic structure, may guide the design and creation of numerous active sites, ultimately enhancing overall activity.

Taking into account these challenges, the fundamental investigation of reaction mechanisms and the elucidation of active sites may be an ongoing pursuit. Concurrently, persistent efforts in optimizing catalyst compositions and structures, especially the exploration of emerging novel catalytic materials, could accelerate the development of more active and selective catalysts. This progress would potentially enable novel processes for synthesizing value-added chemicals and further advance the field.

Author contributions

Conceptualization and supervision: C. Z. and F. W. Investigation, resources, and visualization: G. T., X. L., and H. X. Writing – original draft: G. T., and X. L. Writing – review and editing: G.T., C. Z., and F. W.

Conflicts of interest

There are no conflicts to declare.

Acknowledgements

This work is supported by the National Natural Science Foundation of China (grant no. 22278238, C. Z.), the Key Research and Development Program of Inner Mongolia and Ordos (20211140095, C. Z.), and CNPC Innovation Funds (2020990028, C. Z.).

References

1 J. Li, Y. He, L. Tan, P. Zhang, X. Peng, A. Oruganti, G. Yang, H. Abe, Y. Wang and N. Tsubaki, *Nat. Catal.*, 2018, **1**, 787–793.
2 J. Hu, L. Yu, J. Deng, Y. Wang, K. Cheng, C. Ma, Q. Zhang, W. Wen, S. Yu and Y. Pan, *Nat. Catal.*, 2021, **4**, 242–250.
3 J. Wei, Q. Ge, R. Yao, Z. Wen, C. Fang, L. Guo, H. Xu and J. Sun, *Nat. Commun.*, 2017, **8**, 15174.
4 H.-J. Peng, M. T. Tang, J. Halldin Stenlid, X. Liu and F. Abild-Pedersen, *Nat. Commun.*, 2022, **13**, 1399.

5 Y. Wang, X. Liu, X. Han, R. Godin, J. Chen, W. Zhou, C. Jiang, J. F. Thompson, K. B. Mustafa and S. A. Shevlin, *Nat. Commun.*, 2020, **11**, 2531.
6 B. Zhao, P. Zhai, P. Wang, J. Li, T. Li, M. Peng, M. Zhao, G. Hu, Y. Yang and Y.-W. Li, *Chem*, 2017, **3**, 323–333.
7 F. Jiao, J. Li, X. Pan, J. Xiao, H. Li, H. Ma, M. Wei, Y. Pan, Z. Zhou and M. Li, *Science*, 2016, **351**, 1065–1068.
8 Y. Ni, Z. Chen, Y. Fu, Y. Liu, W. Zhu and Z. Liu, *Nat. Commun.*, 2018, **9**, 3457.
9 R.-P. Ye, J. Ding, W. Gong, M. D. Argyle, Q. Zhong, Y. Wang, C. K. Russell, Z. Xu, A. G. Russell and Q. Li, *Nat. Commun.*, 2019, **10**, 5698.
10 H. Xiong, Z. Liu, X. Chen, H. Wang, W. Qian, C. Zhang, A. Zheng and F. Wei, *Science*, 2022, **376**, 491–496.
11 M. T. Arslan, B. Ali, S. Z. A. Gilani, Y. Hou, Q. Wang, D. Cai, Y. Wang and F. Wei, *ACS Catal.*, 2020, **10**, 2477–2488.
12 M. T. Arslan, B. A. Qureshi, S. A. Gilani, D. Cai, Y. Ma, M. Usman, X. Chen, Y. Wang and F. Wei, *ACS Catal.*, 2019, **9**, 2203–2212.
13 S. Z. A. Gilani, L. Lu, M. T. Arslan, B. Ali, Q. Wang and F. Wei, *Catal. Sci. Technol.*, 2020, **10**, 3366–3375.
14 G. Tian, C. Zhang and F. Wei, *Nanoscale Horiz.*, 2022, **7**, 1478–1487.
15 L. A. Wessjohann, W. Brandt and T. Thiemann, *Chem. Rev.*, 2003, **103**, 1625–1648.
16 X. Pan, F. Jiao, D. Miao and X. Bao, *Chem. Rev.*, 2021, **121**, 6588–6609.
17 L. Zhang, Y. Dang, X. Zhou, P. Gao, A. P. van Bavel, H. Wang, S. Li, L. Shi, Y. Yang and E. I. Vovk, *Innovation*, 2021, **2**, 100170.
18 B. Yao, T. Xiao, O. A. Makgae, X. Jie, S. Gonzalez-Cortes, S. Guan, A. I. Kirkland, J. R. Dilworth, H. A. Al-Megren and S. M. Alshihri, *Nat. Commun.*, 2020, **11**, 6395.
19 K. Cheng, W. Zhou, J. Kang, S. He, S. Shi, Q. Zhang, Y. Pan, W. Wen and Y. Wang, *Chem*, 2017, **3**, 334–347.
20 W. Zhou, C. Zhou, H. Yin, J. Shi, G. Zhang, X. Zheng, X. Min, Z. Zhang, K. Cheng and J. Kang, *Chem. Commun.*, 2020, **56**, 5239–5242.
21 B. Bai, C. Guo, F. Jiao, J. Xiao, Y. Ding, S. Qu, Y. Pan, X. Pan and X. Bao, *Angew. Chem., Int. Ed.*, 2023, e202217701.
22 S. Wang, L. Zhang, P. Wang, W. Jiao, Z. Qin, M. Dong, J. Wang, U. Olsbye and W. Fan, *Nat. Catal.*, 2022, 1–13.
23 Q. Han, P. Gao, K. Chen, L. Liang, Z. Zhao, X. Yao, D. Xiao, X. Han and G. Hou, *Chem*, 2023, **9**, 721–738.
24 W. Zhou, S. Shi, Y. Wang, L. Zhang, Y. Wang, G. Zhang, X. Min, K. Cheng, Q. Zhang and J. Kang, *ChemCatChem*, 2019, **11**, 1681–1688.
25 G. Tian, X. Liu, C. Zhang, X. Fan, H. Xiong, X. Chen, Z. Li, B. Yan, L. Zhang and N. Wang, *Nat. Commun.*, 2022, **13**, 5567.
26 S. Ma, S.-D. Huang and Z.-P. Liu, *Nat. Catal.*, 2019, **2**, 671–677.
27 Z. Zhang, X. Chen, J. Kang, Z. Yu, J. Tian, Z. Gong, A. Jia, R. You, K. Qian and S. He, *Nat. Commun.*, 2021, **12**, 4331.
28 Y. Ji, P. Gao, Z. Zhao, D. Xiao, Q. Han, H. Chen, K. Gong, K. Chen, X. Han and X. Bao, *Nat. Catal.*, 2022, **5**, 594–604.
29 C. Liu, J. Su, S. Liu, H. Zhou, X. Yuan, Y. Ye, Y. Wang, W. Jiao, L. Zhang and Y. Lu, *ACS Catal.*, 2020, **10**, 15227–15237.
30 C. C. Amoo, C. Xing, N. Tsubaki and J. Sun, *ACS Cent. Sci.*, 2022, **8**, 1047–1062.
31 Y. Wang, W. Gao, K. Wang, X. Gao, B. Zhang, H. Zhao, Q. Ma, P. Zhang, G. Yang and M. Wu, *Chem. Sci.*, 2021, **12**, 7786–7792.
32 Z. Huang, S. Wang, F. Qin, L. Huang, Y. Yue, W. Hua, M. Qiao, H. He, W. Shen and H. Xu, *ChemCatChem*, 2018, **10**, 4519–4524.
33 M. T. Arslan, G. Tian, B. Ali, C. Zhang, H. Xiong, Z. Li, L. Luo, X. Chen and F. Wei, *ACS Catal.*, 2022, **12**, 2023–2033.
34 C. Liu, J. Su, Y. Xiao, J. Zhou, S. Liu, H. Zhou, Y. Ye, Y. Lu, Y. Zhang and W. Jiao, *Chem Catal.*, 2021, **1**, 896–907.
35 Z. Li, Y. Qu, J. Wang, H. Liu, M. Li, S. Miao and C. Li, *Joule*, 2019, **3**, 570–583.
36 N. Li, Y. Zhu, F. Jiao, X. Pan, Q. Jiang, J. Cai, Y. Li, W. Tong, C. Xu and S. Qu, *Nat. Commun.*, 2022, **13**, 2742.
37 A. Ramirez, X. Gong, M. Caglayan, S.-A. F. Nastase, E. Abou-Hamad, L. Gevers, L. Cavallo, A. Dutta Chowdhury and J. Gascon, *Nat. Commun.*, 2021, **12**, 5914.
38 W. Zhou, K. Cheng, J. Kang, C. Zhou, V. Subramanian, Q. Zhang and Y. Wang, *Chem. Soc. Rev.*, 2019, **48**, 3193–3228.
39 L. Yang, C. Wang, L. Zhang, W. Dai, Y. Chu, J. Xu, G. Wu, M. Gao, W. Liu and Z. Xu, *Nat. Commun.*, 2021, **12**, 4661.
40 J. Zhou, M. Gao, J. Zhang, W. Liu, T. Zhang, H. Li, Z. Xu, M. Ye and Z. Liu, *Nat. Commun.*, 2021, **12**, 17.
41 Z. Li, J. Wang, Y. Qu, H. Liu, C. Tang, S. Miao, Z. Feng, H. An and C. Li, *ACS Catal.*, 2017, **7**, 8544–8548.
42 J. Gao, C. Jia and B. Liu, *Catal. Sci. Technol.*, 2017, **7**, 5602–5607.
43 S. Dang, S. Li, C. Yang, X. Chen, X. Li, L. Zhong, P. Gao and Y. Sun, *ChemSusChem*, 2019, **12**, 3582–3591.
44 G. Qi, T. E. Davies, A. Nasrallah, M. A. Sainna, A. G. Howe, R. J. Lewis, M. Quesne, C. R. A. Catlow, D. J. Willock and Q. He, *Nat. Catal.*, 2022, **5**, 45–54.
45 C. Zhou, J. Shi, W. Zhou, K. Cheng, Q. Zhang, J. Kang and Y. Wang, *ACS Catal.*, 2019, **10**, 302–310.
46 Y. Wang, W. Gao, S. Kazumi, H. Li, G. Yang and N. Tsubaki, *Chem. – Eur. J.*, 2019, **25**, 5149–5153.
47 W. Gao, L. Guo, Y. Cui, G. Yang, Y. He, C. Zeng, A. Taguchi, T. Abe, Q. Ma and Y. Yoneyama, *ChemSusChem*, 2020, **13**, 6541–6545.
48 N. Li, F. Jiao, X. Pan, Y. Chen, J. Feng, G. Li and X. Bao, *Angew. Chem., Int. Ed.*, 2019, **58**, 7400–7404.
49 S. Müller, Y. Liu, M. Vishnuvarthan, X. Sun, A. C. van Veen, G. L. Haller, M. Sanchez-Sanchez and J. A. Lercher, *J. Catal.*, 2015, **325**, 48–59.
50 D. Laudenschleger, H. Ruland and M. Muhler, *Nat. Commun.*, 2020, **11**, 3898.
51 H. Zhao, R. Yu, S. Ma, K. Xu, Y. Chen, K. Jiang, Y. Fang, C. Zhu, X. Liu and Y. Tang, *Nat. Catal.*, 2022, **5**, 818–831.
52 Y. Liu, F. M. Kirchberger, S. Müller, M. Eder, M. Tonigold, M. Sanchez-Sanchez and J. A. Lercher, *Nat. Commun.*, 2019, **10**, 1462.